Supporting Information

From High Loading to High Activity: Unraveling the Correlation in High Performance Single-Atom Catalysts Design

Degao Zhang[a], Qian Lin[a], Guangjun Nan[b], Yi zhang[a], Dawei Fu[a], Liyan Xie[,a]*

a. Institute for Science and Applications of Molecular Ferroelectrics, Key Laboratory of the Ministry of Education for Advanced Catalysis Materials, Zhejiang Normal University, Jinhua, 321004, P. R. China.

b. Department of Physics, Zhejiang Normal University, Jinhua, Zhejiang 321004, P. R. China.

**Corresponding author.*

E-mail: liyanxie@zjnu.edu.cn

In the Electronic Supplementary Material section, the following parts are included:

1. Calculation Details

The binding energy of a single TM atom ($E_{b,mono}$), binding energy of a TM dimer ($E_{b,di}$), adsorption energy (ΔE), and clustering energy ($E_{cluster}$) were computed using the following equations.

$$E_{b,mono} = (E_{TM-GY} - E_{GY} - nE_{TM}) / n \qquad (n = 1, 2) \qquad (1)$$

$$E_{b,di} = (E_{2TM-GY} - E_{GY} - 2E_{TM}) / 2 \qquad (2)$$

$$\Delta E = E_{X@TM-GY} - E_{TM-GY} - E_X \qquad (X = O, OH, OOH) \qquad (3)$$

$$E_{cluster} = E_{b,mono} - E_{b,di} \qquad (4)$$

Where E_{GY}, E_{TM}, and E_{TM-GY} are the energies of the pristine GY, isolated TM atoms, and GY adsorbing TM atoms, respectively, while n denotes the number of adsorbed TM atoms. E_{2TM-GY} corresponds to the energy of GY with an adsorbed TM dimer. $E_{X@TM-GY}$ and E_X denote the energy of the catalyst adsorbing X species and the energy of isolated X in the gas phase, respectively. $E_{cluster}$ quantifies the binding energy

difference between single TM atoms and dimers on the surface. When $E_{cluster}$ is negative – indicating higher stability for single-atom adsorption than dimer adsorption – aggregation of single atoms is thermodynamically suppressed [1, 2].

Using Nørskov's electrocatalytic framework [3], we simulate acidic (pH = 0) water splitting at active sites via four elementary steps, as follows:

$H_2O + * \rightarrow *OH + H^+ + e^-$

$*OH \rightarrow *O + H^+ + e^-$

$*O + H_2O \rightarrow *OOH + H^+ + e^-$

$*OOH \rightarrow * + O_2 + H^+ + e^-$

Where * is the active site of the catalyst, and *OH, *O, and *OOH corresponding three reaction intermediates.

The Gibbs free energy change (ΔG) was calculated at each reaction step as follows [4]:

$$\Delta G = \Delta E + \Delta ZPE - T\Delta S + \Delta G_U - \Delta G_{pH} \quad (5)$$

Where ΔE represents the total energy change derived from DFT simulations. The ΔZPE and ΔS values obtained from frequency calculations represent the zero-point energy correction and entropy correction at 298.15 K and 1 bar, respectively. Note that water's reference state at this temperature is 0.035 bar, corresponding to the liquid-vapor equilibrium condition. The electrode potential contribution to Gibbs free energy follows $\Delta G_U = -eU$, with U defined vs RHE. $\Delta G_{pH} = 0.059 \times pH$. Given the condition pH = 0 in this study, this term evaluates to zero.

To quantify catalytic activity, the OER overpotential of catalysts can be calculated using [5]:

$$\eta = \max [\Delta G_1, \Delta G_2, \Delta G_3, \Delta G_4] / e - 1.23\ V \quad (6)$$

where 1.23 V is the potential for an ideal OER catalyst at pH = 0.

2. Figures

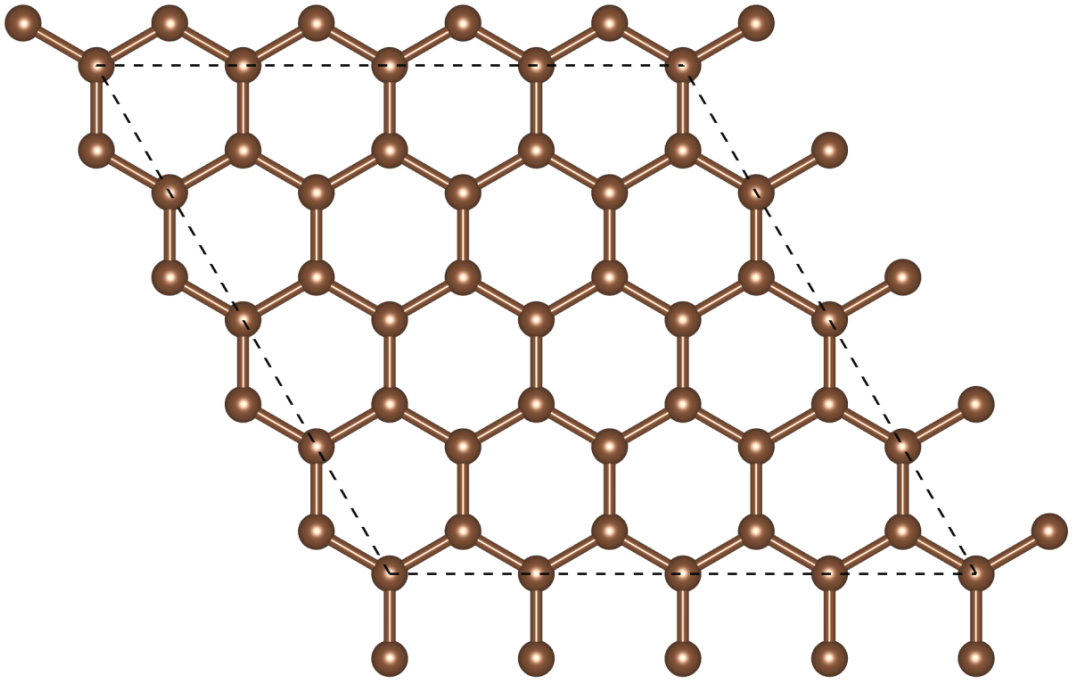

Figure S1. Atomic structure of the 4×4 graphene supercell.

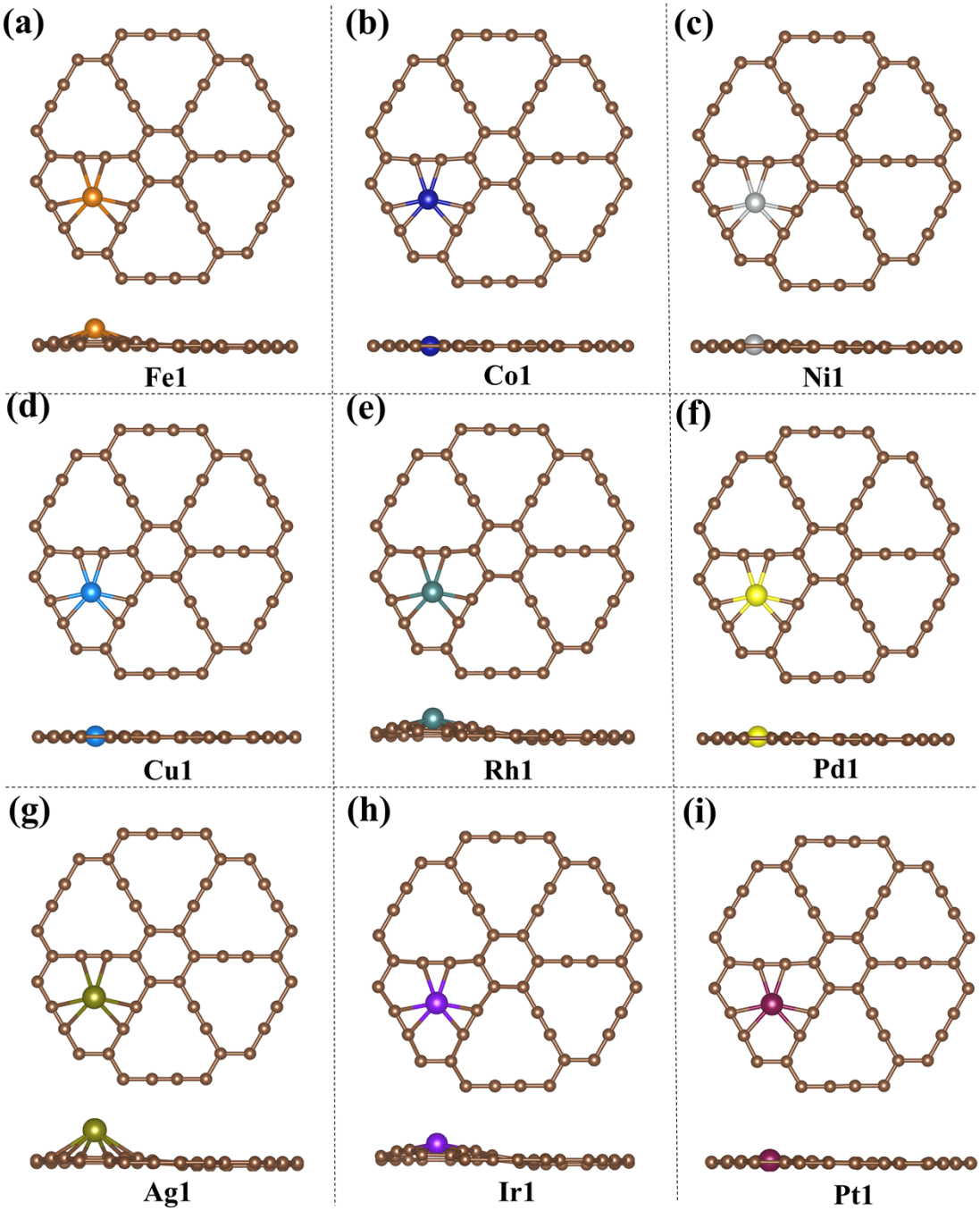

Figure S2. (a-i) Top and side views of the optimized atomic structures of low-loading TM-GY (TM = Fe, Co, Ni, Cu, Rh, Pd, Ag, Ir, and Pt).

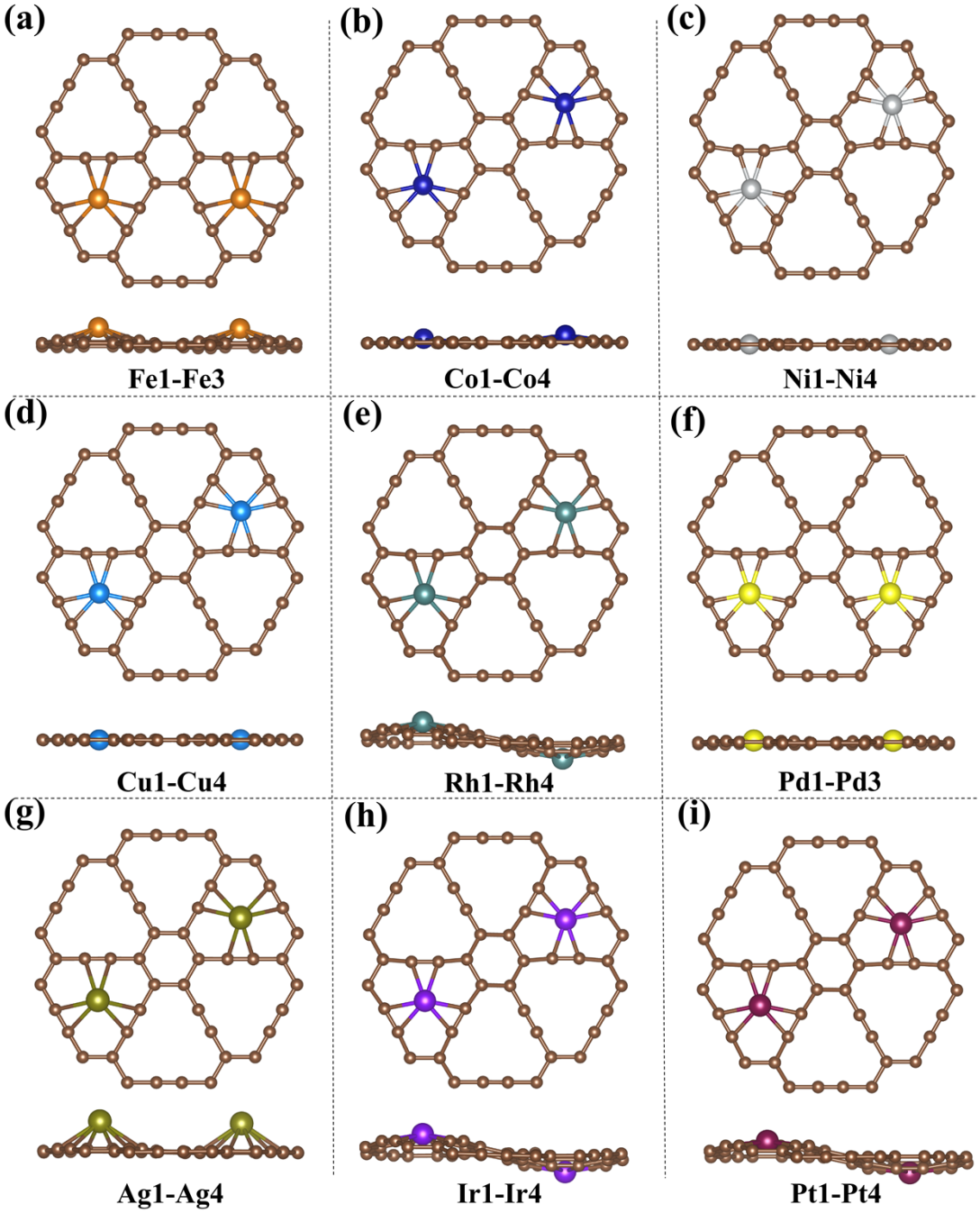

Figure S3. (a-i) Top and side views of the optimized atomic structures of high-loading TM-GY (TM = Fe, Co, Ni, Cu, Rh, Pd, Ag, Ir, and Pt).

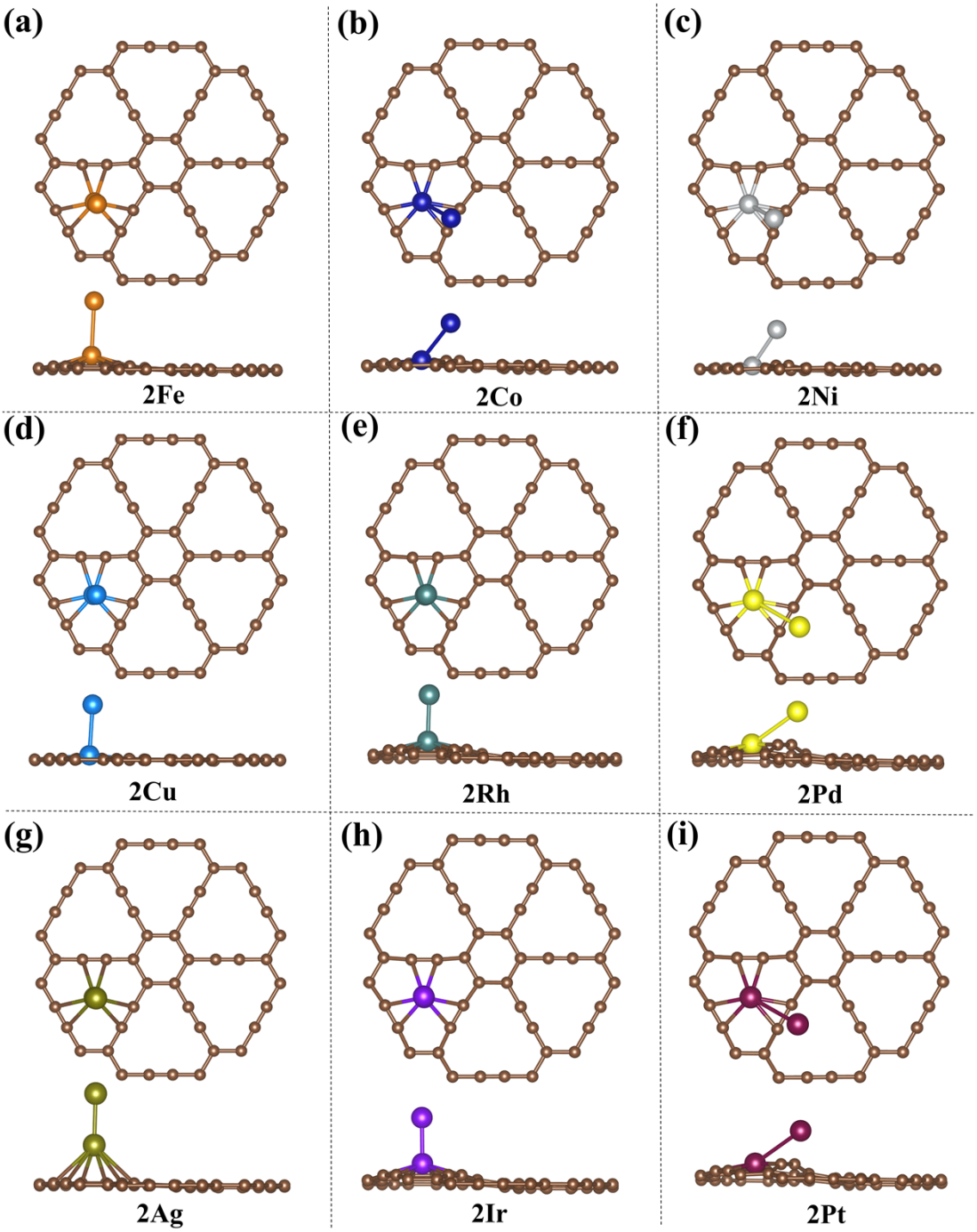

Figure S4. (a-i) Top and side views of optimized atomic structures for TM dimers (TM = Fe, Co, Ni, Cu, Rh, Pd, Ag, Ir, and Pt) adsorbed on GY surfaces.

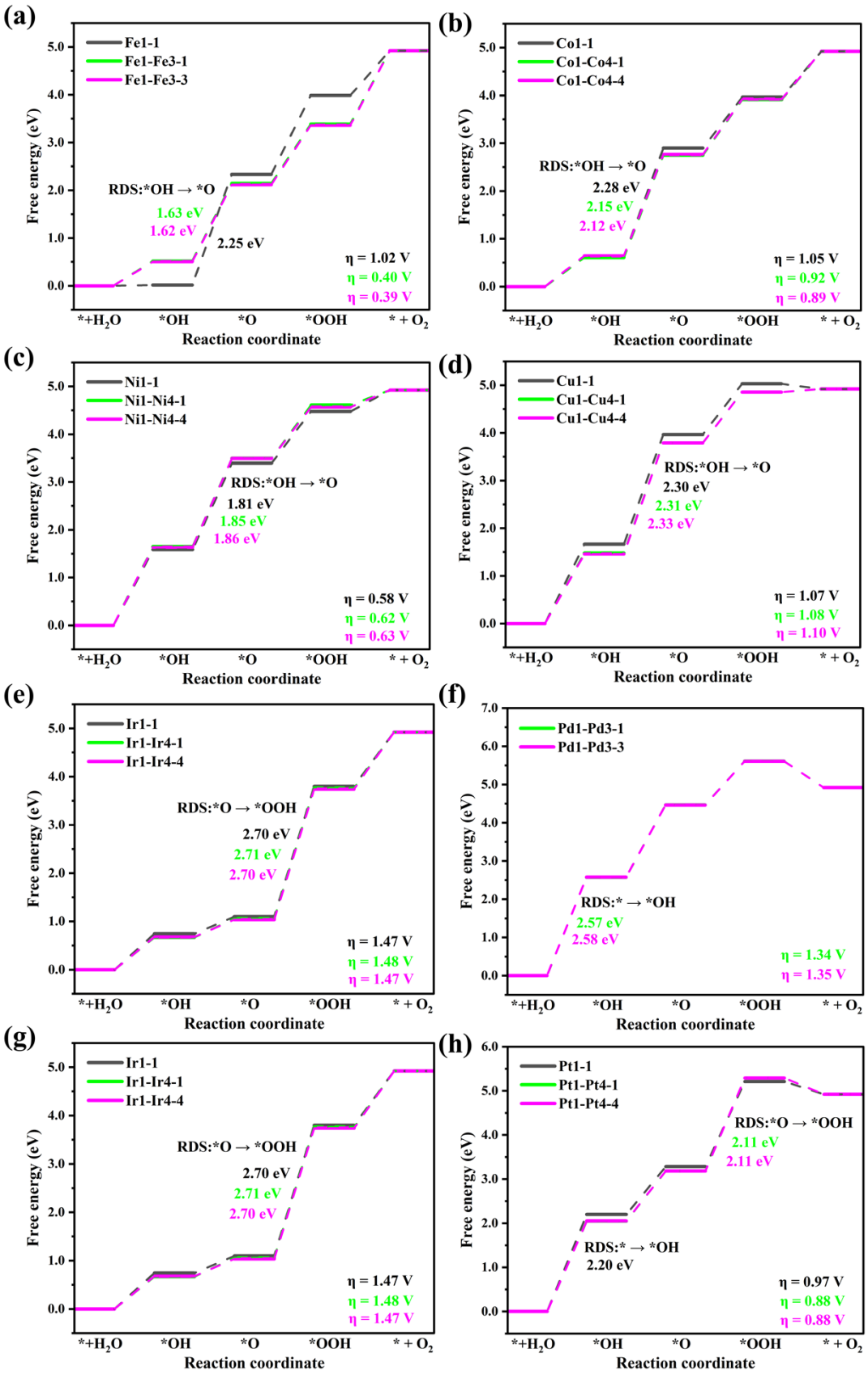

Figure S5. (a-h) OER Gibbs free energy diagrams and overpotentials of low- and high-loading TM-GY (TM = Fe, Co, Ni, Cu, Rh, Pd, Ir, and Pt). The numerals 1, 3 and 4 denote the TM site labeling.

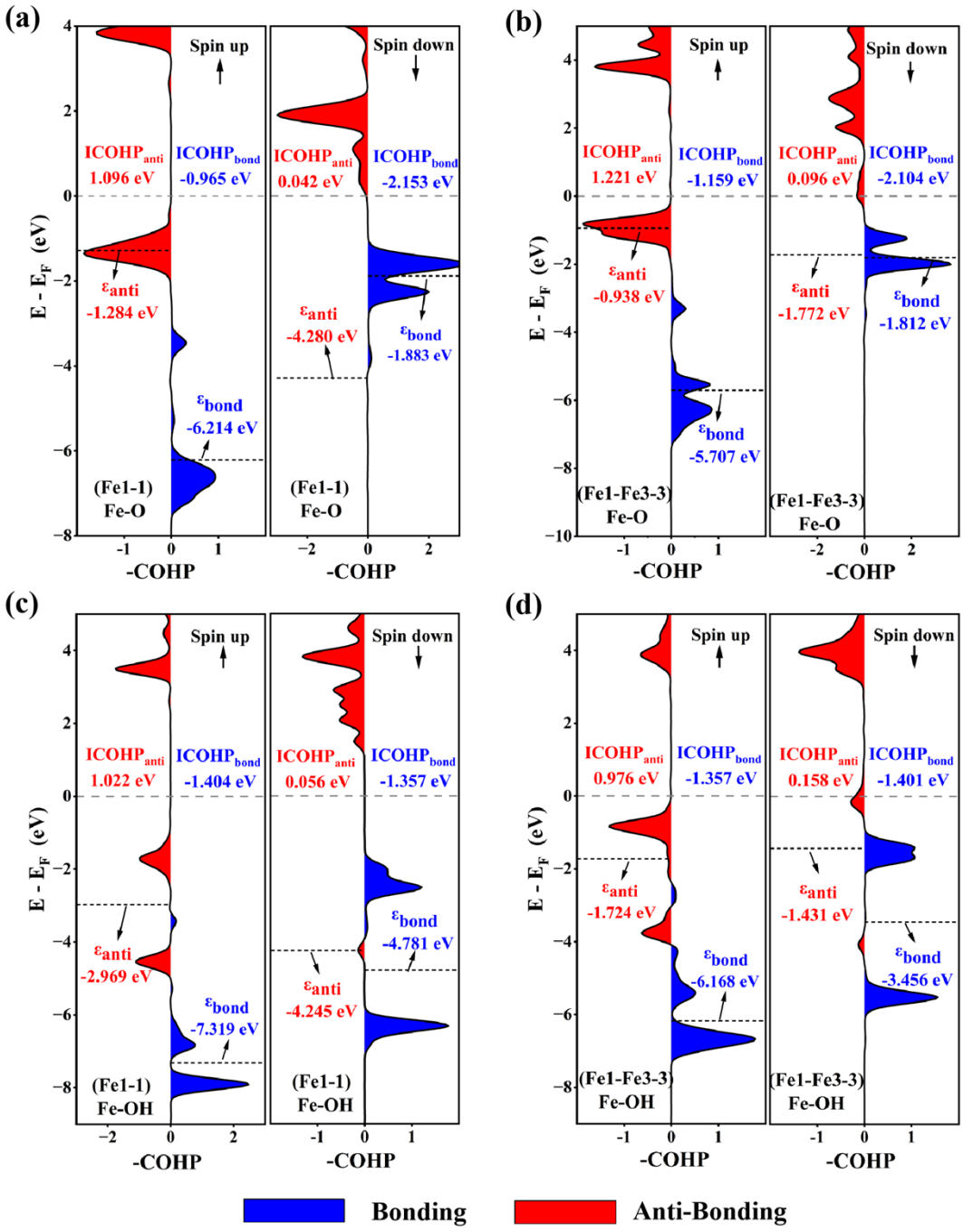

Figure S6. Spin-polarized COHP analysis for Fe-O bond : (a) *O at Fe1-1 site, (b) *O at Fe1-Fe3-3 site, (c) *OH at Fe1-1 site, and (d) *OH at Fe1-Fe3-3 site. The numerals 1, and 3 denote the TM site labeling.

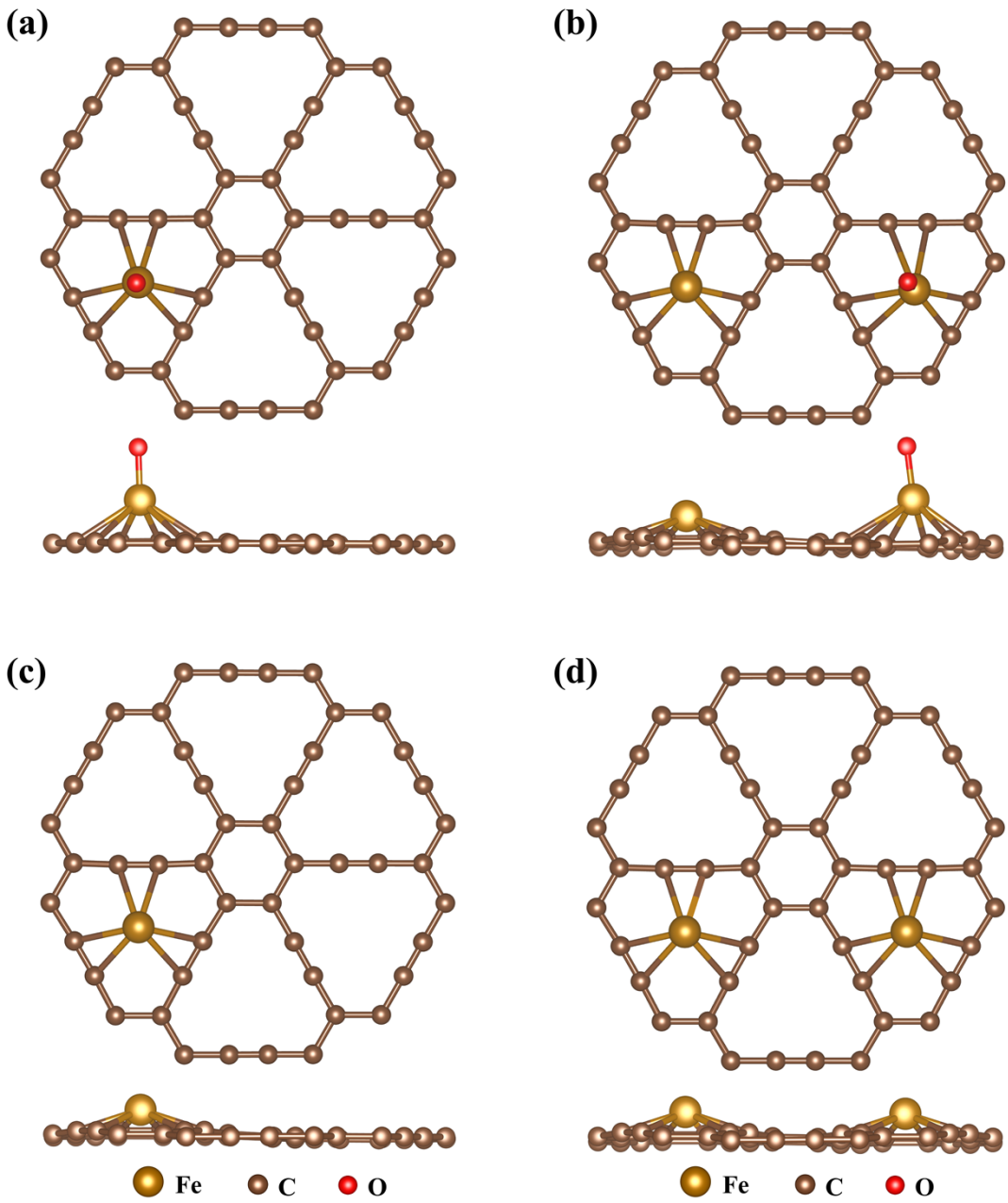

Figure S7. Side and top views of the optimized structures: (a) *O on Fe1-1 (b) *O on Fe1-Fe3-3 (c) Fe1 (d) Fe1-Fe3.

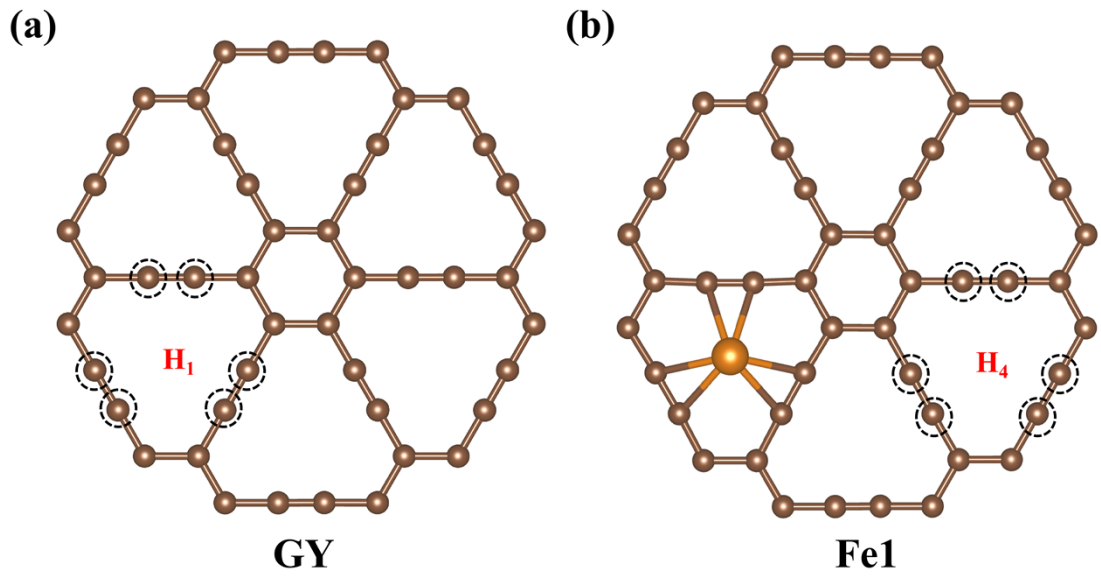

Figure S8. The carbon atoms represented by (a) GY-H1 and (b) Fe1-H3 in Figure S9.

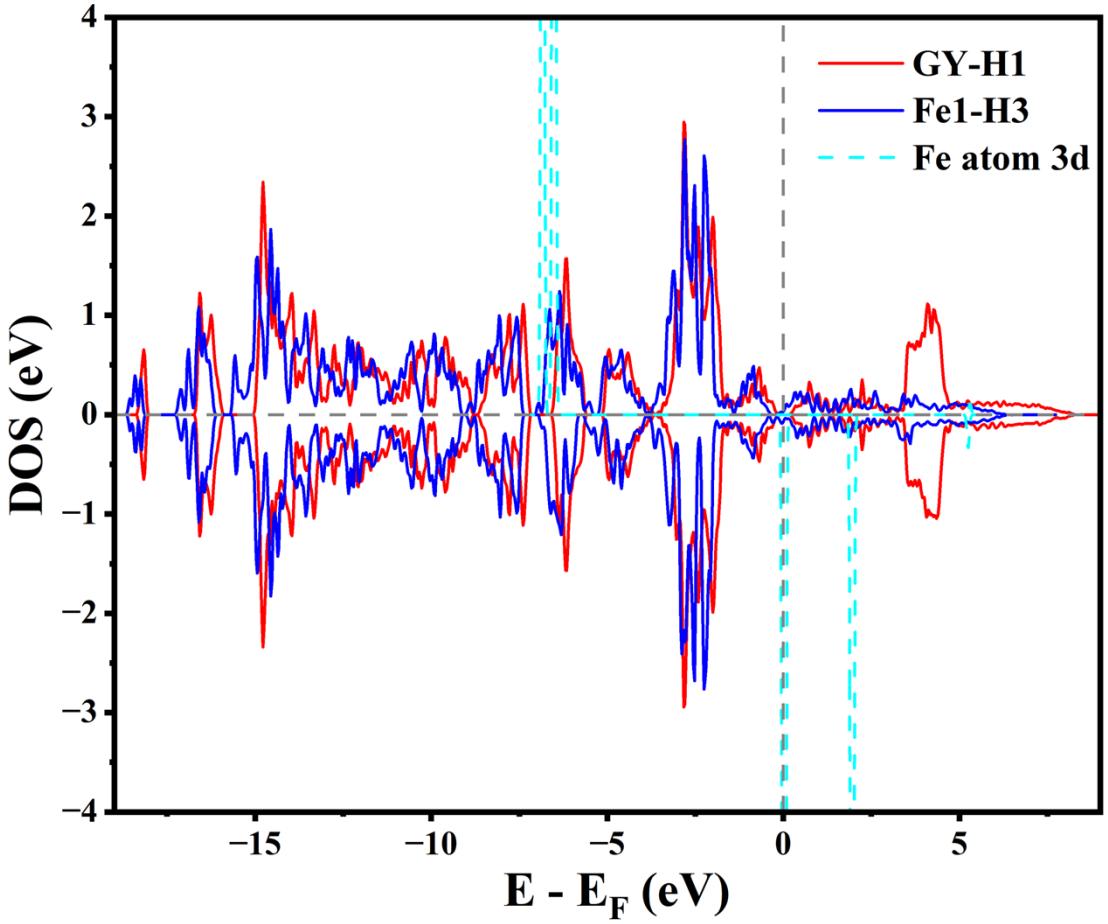

Figure S9. The density of states (DOS) for GY-H1, Fe1-H3, and Fe atom 3d.

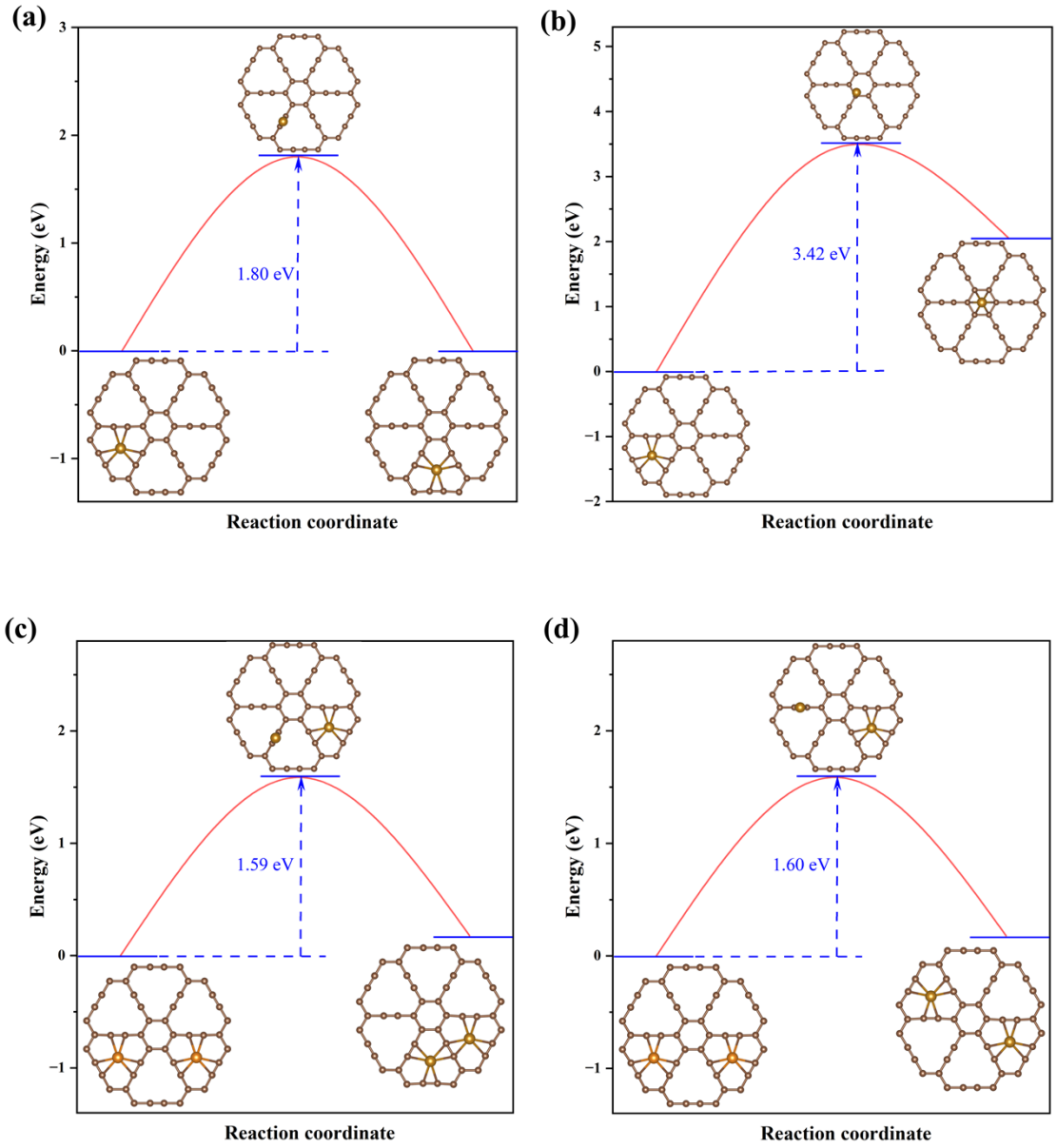

Figure S10. Energy change during Fe atom diffusion process: (a–b) low-loading Fe-GY and (c–d) high-loading Fe-GY.

Table S1. From top to bottom, the values are (in eV): the energies of the three possible configurations of high-loading TM-GY, the energy of GY with an adsorbed TM dimer, and the binding energy and clustering energy of TM atoms for the most stable high-loading TM-GY.

TM	Fe	Co	Ni	Cu	Rh	Pd	Ag	Ir	Pt
$E_{\mathrm{TM1\text{-}TM2}}$	-422.72	-419.47	-418.12	-415.98	-418.50	-421.33	-414.97	-424.11	-421.40
$E_{\mathrm{TM1\text{-}TM3}}$	-422.91	-419.88	-418.52	-416.36	-418.37	-421.40	-415.03	-424.04	-421.33
$E_{\mathrm{TM1\text{-}TM4}}$	-422.85	-420.16	-418.56	-416.42	-418.56	-421.23	-415.07	-424.37	-421.55
$E_{\mathrm{2TM\text{-}GY}}$	-421.28	-417.99	-416.62	-414.04	-417.75	-420.23	-415.22	-422.37	-420.24
$E_{\mathrm{b,mono}}$	-1.38	-1.59	-1.94	-1.20	-1.02	-3.78	-0.57	-3.92	-3.42
E_{cluster}	-0.75	-1.08	-0.96	-1.19	-0.41	-0.58	0.05	-1.00	-0.66

References

[1] Ghosh, D.; Periyasamy, G.; Pandey, B.; Pati, S. K. Computational studies on magnetism and the optical properties of transition metal embedded graphitic carbon nitride sheets. *J. Mater. Chem. C* **2014**, *2*, 7943-7951.

[2] Chen, M.; Zhao, Y.-J.; Liao, J.-H.; Yang, X.-B. Transition-metal dispersion on carbon-doped boron nitride nanostructures: Applications for high-capacity hydrogen storage. *Phys. Rev. B* **2012**, *86*, 045459.

[3] Rossmeisl, J.; Qu, Z. W.; Zhu, H.; Kroes, G. J.; Nørskov, J. K. Electrolysis of water on oxide surfaces. *J. Electroanal. Chem.* **2007**, *607*, 83-89.

[4] Norskov, J. K.; Rossmeisl, J.; Logadottir, A.; Lindqvist, L.; Kitchin, J. R.; Bligaard, T.; Jonsson, H. Origin of the Overpotential for Oxygen Reduction at a Fuel-Cell Cathode. *J. Phys. Chem. B* **2004**, *108*, 17886-17892.

[5] Man, I. C.; Su, H. Y.; Calle-Vallejo, F.; Hansen, H. A.; Martínez, J. I.; Inoglu, N. G.; Kitchin, J.; Jaramillo, T. F.; Nørskov, J. K.; Rossmeisl, J. Universality in Oxygen Evolution Electrocatalysis on Oxide Surfaces. *ChemCatChem* **2011**, *3*, 1159-1165.